Q. J. R. Meteorol. Soc. (0000), **000**, pp. 1–999

The Annual Cycle of Persistence in the El Niño-Southern Oscillation

By CHRISTOPHER TORRENCE[1]* and PETER J. WEBSTER[1]

[1] *Program in Atmospheric and Oceanic Sciences, University of Colorado at Boulder, Boulder, Colorado.*

(QJ 96/164, submitted 25 October 1996, revised 14 June 1997, second revision 19 December 1997)

FINAL DRAFT

SUMMARY

A spring "predictability barrier" exists in both data and models of the El Niño-Southern Oscillation (ENSO) phenomenon. In statistical analyses this barrier manifests itself as a drop-off in monthly persistence (lagged correlation) while in coupled ocean-atmosphere models it appears as a decrease in forecast skill.

The persistence barrier for ENSO indices is investigated using historical sea surface temperature and sea level pressure data. Simple statistical models are used to show that the persistence barrier occurs because the boreal spring is the transition time from one climate state to another, when the "signal-to-noise" of the system is lowest and the system is most susceptible to perturbations. The strength of the persistence barrier is shown to depend on the degree of phase locking of the ENSO to the annual cycle.

The phase locking of the ENSO to the annual cycle, as well as the ENSO variance, is shown to vary on interdecadal time scales. During 1871–1920 and 1960–1990 the ENSO variance was high, while during 1920–1950 the ENSO variance was low. Using wavelet analysis, this interdecadal variability in ENSO is shown to be correlated with changes in Indian summer monsoon strength. Finally, the change in persistence barrier strength between 1960–1979 and 1980–1995 is related to changes in the phase locking of ENSO to the annual cycle. These changes in persistence and phase locking appear to be related to the increased forecast skill seen in recent coupled ocean-atmosphere models.

KEYWORDS: El Niño-Southern Oscillation   Predictability   Interdecadal Variability

1. INTRODUCTION

During the 1930's, Sir Gilbert Walker outlined the characteristics of the "Southern Oscillation", consisting of a global-scale "see-saw" of pressure, rainfall, and temperature anomalies centered on the tropical Pacific Ocean (Walker and Bliss 1932, 1937). Walker's attempts to "foreshadow" the strength of the Indian summer monsoon were based on both the high correlations of his "Southern Oscillation Index" (SOI) with the Indian monsoon, and on the seasonal persistence of the oscillation. Unfortunately, Walker discovered that the persistence in the SOI is much higher *following* the June–August monsoon season, than preceding the monsoon. Furthermore, the correlations between the Southern Oscillation and the Indian monsoon decreased considerably after about 1925, leading to speculation that whatever usefulness Walker's model might have possessed was now gone (Normand 1953; Treloar and Grant 1953).

After a thirty-year quiescent period, both in research and in Indian monsoon and Southern Oscillation variability, Troup (1965) re-examined the evidence and found that while there had been some secular changes since 1920, all of Walker's earlier correlations remained valid. Walker's index still showed large persistence from season to season, with the least persistence across the March–May season. In examining this seasonal change in persistence, Walker and Bliss (1932) concluded that "*conditions in the southern winter exercised greater influence on subsequent seasons than did those in the southern summer.*"

Much of the research in the last thirty years has been on analyzing the Southern Oscillation as part of the larger El Niño-Southern Oscillation (ENSO) phenomenon, involving basin-wide migrations of both pressure and sea surface temperature (SST) anomalies (Rasmusson and Carpenter 1982). The recognition of the ENSO as a coupled

* Corresponding author: Advanced Study Program, National Center for Atmospheric Research, P.O. Box 3000, Boulder CO 80307–3000, USA..

ocean-atmosphere phenomenon has enabled the development of simple models capable of useful predictions up to nine months in advance (Cane *et al.* 1986).

Unfortunately, many of these models suffer from a decrease in forecast skill in the boreal spring months of March–May (Barnston *et al.* 1994). This "predictability barrier" has been found in an oceanic general circulation model (Latif and Graham 1991), in dynamical-statistical models (Balmaseda *et al.* 1994), and in coupled ocean-atmosphere models (Goswami and Shukla 1991; Xue *et al.* 1994).

The predictability barrier has been attributed to the low variance of the ENSO during the spring (Xue *et al.* 1994). During the spring, errors due to initialization or "weather" can project most strongly onto ENSO modes, leading in turn to large error growth and poor forecasts (Blumenthal 1991; Moore and Kleeman 1996). It has been suggested that the inclusion of external influences such as the Asian monsoon may help to "bridge" the barrier (Webster and Yang 1992), but the results are tenuous at best (Lau and Yang 1996). Recent model results by Chen *et al.* (1995, 1997) also suggest that a coupled initialization procedure is able to reduce the barrier.

Rather than view the spring barrier as a failure of the models, it is noted that a similar drop-off is seen in the persistence of ENSO indices (Wright 1985; Webster 1995). First noticed by Walker and Bliss (1932), the "persistence barrier" has been found in indices of central Pacific rainfall (Wright 1979), Atlantic SST (Wright 1987), the SOI (Troup 1965; Webster and Yang 1992), as well as Pacific SST (Xue *et al.* 1994).

The purpose of this paper is to examine in detail the persistence barrier for the El Niño-Southern Oscillation, and discuss the relationship between the persistence barrier and model forecast skill.

Section 2 discusses the datasets. Section 3 gives background results on the persistence barrier, while Section 4 provides statistical models to explain the persistence barrier in ENSO indices, and introduces the signal-to-noise ratio. The spatial extent of the persistence barrier is also discussed. Section 5 examines changes in variance and persistence on interdecadal time scales. Section 6 relates the persistence barrier and interdecadal changes to ENSO forecast skill. A summary is given in Section 7.

2. Data

The Southern Oscillation Index (SOI) is traditionally defined as the standardized difference between the standardized Tahiti (17.6°S 149.6°W) and Darwin (12.4°S 130.9°E) sea level pressure (SLP) (Trenberth 1984). However, missing data in the Tahiti record make it difficult to extend the SOI back before 1933. (Ropelewski and Jones 1987). To overcome this difficulty, an alternate measure of the SOI will be used, based on the UKMO/CSIRO historical sea level pressure (SLP) dataset (GMSLP2.1f, on a 5°-grid, monthly 1871–1994; courtesy D. Parker and T. Basnett, Hadley Centre for Climate Prediction and Research, UKMO, UK). Anomaly time series have been constructed by removing the first three harmonics of the annual cycle (365.25, 182.623, and 121.75 days) using a least-squares fit. The SOI from the GMSLP is defined as the seasonally-averaged pressure difference between the eastern Pacific (at 20°S, 150°W) and the western Pacific (at 10°S, 130°E). This SOI has about 20% less variance than the Tahiti-Darwin SOI, but does not contain any missing data, and also extends further back in time. Henceforth, the term SOI will refer to this GMSLP-derived index.

The Indian monsoon strength is derived from the all-India RF1 rainfall index given in Parthasarathy *et al.* (1991). The index is defined as the deviations from the normal rainfall for June–September, and is available from 1871–1994. For details of the all-India index and its relation to regional rainfall anomalies, see Mooley and Parthasarathy (1984).

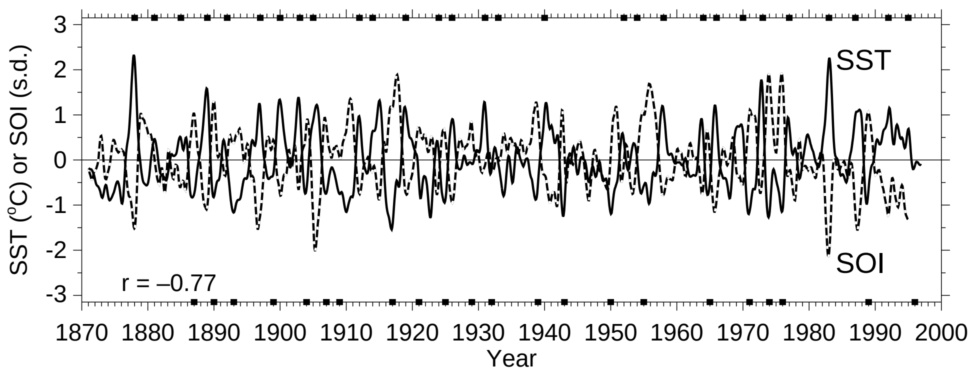

Figure 1. Time series of NINO3 SST (solid line, units in °C) and the SOI (dashed line, units in standard deviations). For presentation purposes, both time series have been smoothed by an 11–month Lanczos filter (Trenberth 1984). The black marks on the top axis mark starting years of El Niño events, while those on the bottom axis mark La Niña events, as defined by Kiladis and Diaz (1989).

Gridded monthly sea surface temperature (SST) data for 1871–1996 is from the UK Meteorological Office GISST2.3 (Rayner *et al.* 1996). The quality of gridded SST data between 1871–1950 varies considerably both spatially and temporally. Ship data before 1900 is sparse, especially for the Southern Hemisphere. After 1900 the data coverage increases, except for World Wars I and II. Around 1940 many ships changed from bucket measurements of temperature to ship intake, causing discontinuities on the order of 0.3°C. The GISST dataset attempts to correct for all of these biases by using the existing data to construct Empirical Orthogonal Functions (EOF), and then projecting these modes onto the available data. A discussion of the technique is given in Rayner *et al.* (1996), while a general discussion of data-quality issues for ship SST measurements is found in Folland *et al.* (1984).

The NINO3 SST index is defined as the area-averaged GISST over the central Pacific (5°S–5°N, 90°W–150°W). Monthly anomalies are computed with respect to the annual cycle of the entire time series.

Smoothed versions of both the NINO3 SST and the SOI are shown in Figure 1, where one can see the strong anti-correlation between the two ($r = -0.77$ for the smoothed time series). The black marks indicate warm ENSO events (top axis) or cold ENSO events (bottom axis), as defined by Kiladis and Diaz (1989). There is large variability in the amplitude, duration, and frequency of ENSO events, with very strong events such as the 1982–83 El Niño as well as the long-lasting 1991–1995 "warm event". There are hints of interdecadal variability, with an active period in the early 1900's followed by a relatively quiet period during the 1920's–1950's followed by the most recent active period. In the next section the persistence and phase locking of the time series (unsmoothed) will be discussed.

3. ENSO Indices

In this section, the autocorrelation, persistence, and phase locking of the El Niño-Southern Oscillation are examined. Results in these subsections are based primarily upon the work of Trenberth (1984), Webster and Yang (1992), and Rasmusson and Carpenter (1982).

(a) *Autocorrelation*

The "autocorrelation" is the correlation of an entire time series with itself, only shifted in time by a certain lag. Both the SST and the SOI show a slow drop-off of autocorrelation (c.f. Trenberth 1984). The SST autocorrelation (not shown) reaches the limit of "useful skill" of $r = 0.6$ (Barnston *et al.* 1994) after four months and crossing the zero line after 12 months. The high degree of autocorrelation in both indices is consistent with the observation that ENSO anomalies tend to persist for several months, and suggests that one can gain useful information from a forecast of simple persistence out to several months. However, as shown in the next subsection, this is not true for every month. The starting month of a persistence forecast plays a crucial role in the success or failure of the prediction.

(b) *Persistence*

Following Troup (1965), the "persistence" is defined as the fixed-phase correlation between different months of a single time series. The persistence from January to July in the SOI is the correlation coefficient between all January SOI values and all July SOI values (see Appendix for formula). Unlike the autocorrelation, which is independent of starting month, the persistence returns information about any seasonal changes in the correlation between one month and the next.

Figures 2a and 2b shows the persistence for the NINO3 SST and the SOI time series, and is similar to plots in Webster and Yang (1992) and Wright (1985). Unlike the simple decay of the autocorrelation, the persistence shows a distinct structure that is phase locked to the annual cycle. The persistence drops off more slowly for late spring and summer starts, followed by sharp drop-offs during the following March–April. Note that the persistence barrier can also be seen in the lag-1 persistence (the black dots) as a minimum in June (SST) or April (SOI).

In the persistence maps (Figs. 2c and 2d) the drop-off appears as a vertical alignment of contours centered on March-April-May. Compared to the NINO3 SST, the SOI shows a less well-defined barrier due to high-frequency noise, which also appears in the lower lag-1 persistences for the SOI. Beyond twelve months, the SST and SOI persistences are slightly negative, possibly due to the biennial nature of ENSO: of the 29 warm ENSO events since 1877, ten were followed the next year by cold events. Plots of the root-mean-square (RMS) error for persistence forecasts (not shown) give a similar persistence barrier. For RMS error, the barrier appears as a sudden increase in error during spring, regardless of starting month.

There are two main observations for the NINO3 SST and SOI persistences:

(i) Regardless of starting month, the persistence in ENSO indices is consistently high through the following March, and,
(ii) Regardless of starting month, the persistence shows a rapid decline in March-April-May.

In the next subsection a hypothesis will be given to explain the existence of a persistence barrier within a time series.

(c) *Phase Locking of ENSO*

It is well known that many ENSO events are phase locked to the annual cycle (Rasmusson and Carpenter 1982), although the degree of phase locking may vary from decade to decade (see Section 5). A composite of the NINO3 SST index for the last 29 warm ENSO events and 22 cold ENSO events is shown in Fig. 3. Both warm and cold

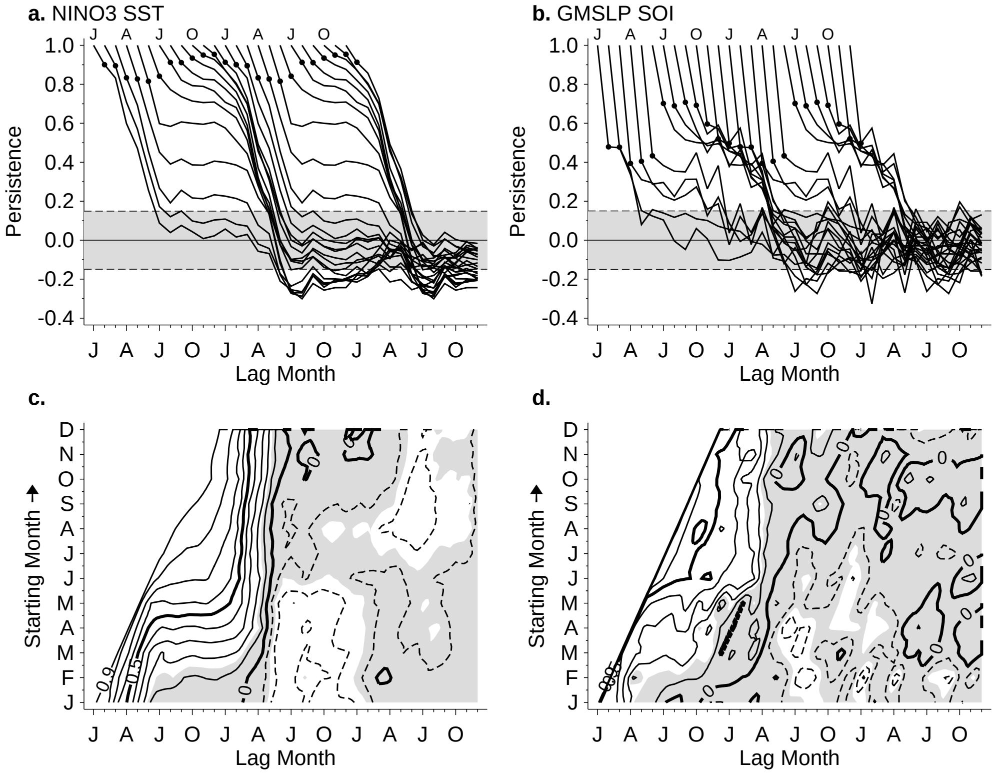

Figure 2. (a) Persistence of the NINO3 SST. Each curve has been shifted to line up the starting month (indicated at the top, where JAJO=January, April, July, October) with the corresponding lag month (lower axis), and the twelve curves have been repeated for clarity. The black dots show the lag-1 persistence. (b) Same as (a) but for the SOI. (c) Same information as (a) but viewed as a persistence "map" with starting month along the y-axis. The contours are every 0.1, with thick contours at 0.0 and 0.5. (d) Same as (c) but for the SOI. In all plots, the shaded region indicates less than 95% confidence for Student's-t test with 121 degrees of freedom.

events begin as anomalies of the opposite sign in year (−1), cross the zero-anomaly line around March of year (0), and peak in the following winter.

The ENSO cycle is confirmed by global composites of wind fields and SST (Rasmusson and Carpenter 1982) as well as outgoing-longwave radiation and precipitation (Meehl 1987). The biennial nature of ENSO can be seen as the tendency for warm events to be followed by cold anomalies, and the even larger tendency for cold events to be preceded by warm anomalies. The analysis by Barnett (1991) of the quasi-biennial component (20–30 months) of winds along the equator (using data from 1950–1988), shows phase locking to the annual cycle, with roughly 50% of the zero-crossings occurring during February–April.

Using the composite ENSO in Fig. 3 as a guide, and paralleling the observations at the end of Section 3b, the following hypothesis is proposed:

(i) The persistence is consistently high during May–January due to the slow, steady growth of ENSO events, and,
(ii) The persistence drops off in the boreal spring due to the low signal-to-noise of ENSO relative to the background. This low signal-to-noise is a result of the strong phase locking of ENSO to the annual cycle, which causes the time of transition between

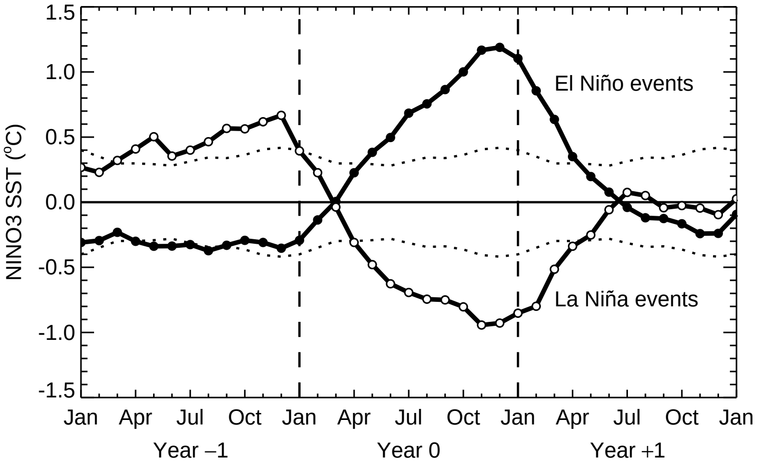

Figure 3. Composite of the 29 El Niño events and 22 La Niña events occuring between 1877–1995, as defined by Kiladis and Diaz (1989). The composite is the mean of monthly SST anomalies for all warm events (solid dots) or cold events (open dots). Year 0's are defined as in Rasmusson and Carpenter (1982). Dotted lines mark the 95% confidence levels for a mean of 22 points taken from a population with the monthly-varying standard deviations of the entire NINO3 SST time series.

ENSO events to occur in the spring.

Note that a persistence barrier does not necessarily imply a loss of actual predictability. Looking at Fig. 3, it might appear that if one knew the winter–spring trend in NINO3 SST, then one could predict SST anomalies in the following winter. However, Fig. 3 is a composite over only anomalously warm and cold years, and thus has the advantage of hindsight. Indeed, a correlation of trend from winter to spring on the months following spring shows only a small skill improvement (≈ 0.1) compared with the persistence in Fig. 2. In addition, during winter-to-spring, the annual cycle in the eastern Pacific shows a warming trend, making it difficult to distinguish potential warm events from possibly random fluctuations in the amplitude or phase of the annual cycle.

4. The Persistence Barrier

In this section, two different statistical models are developed to explain the persistence barrier in ENSO indices. These models are then analyzed in terms of the annual cycles of their signal-to-noise ratios. The spatial extent of the persistence barrier is then examined using global SST fields.

(*a*) *Autoregressive Model*

The hypothesis in the previous section will be tested using the persistence of several time series. As the persistence is defined in terms of a fixed-phase correlation, the most natural model to consider is a simple autoregressive (AR) equation:

$$X_t = \alpha_m X_{t-1} + Z_t, \tag{1}$$

where X represents an ENSO index such as the NINO3 SST and the subscript t is the time measured in months starting from year zero. It is assumed that $X_0 = 0$, and the model is then integrated forward by successively substituting in previous X values and new Z values. The AR coefficient, α_m, may depend on the month m. Finally, Z_t is drawn from twelve Gaussian white noise processes of zero mean and variances σ^2_{Zm}, where m indicates the month.

The fixed-phase persistence for (1) can be derived analytically (see Appendix), and is given by,

$$P_m(k) = \frac{\sigma_m}{\sigma_{m+k}} \prod_{j=1}^{k} \alpha_{m+j}, \tag{2}$$

where the subscript m indicates the starting month, k is the lag in months, and σ_m is the standard deviation of X_t for the m-th month (see Appendix for equation). The persistence from one month (m) to another (k months in the future) depends on the ratio of the standard deviations of the two months, and the product of the AR coefficients between $m+1$ and $m+k$, as each successive month decreases the persistence from the previous month.

In an attempt to simulate the persistence barrier using (1), several cases will now be considered.

(i) *Constant AR coefficients and constant noise variance*
For $\alpha_m = \alpha$ and $\sigma_{Zm} = \sigma_Z$, the persistence in (2) becomes $P_m(k) = \alpha^k$. This persistence is independent of starting month and cannot produce a persistence barrier.

(ii) *Constant AR coefficients and varying noise variance*
Now, $\alpha_m = \alpha$, while σ_{Zm} is allowed to vary with month, and the persistence is given by $P_m(k) = \alpha^k \sigma_m / \sigma_{m+k}$. In this case, a drop in variance during the forecast season (say the boreal spring) will actually cause an increase in persistence, due to the small amplitude of the signal being predicted. Since this is not observed, the persistence barrier in ENSO cannot be explained solely by an annual cycle in the noise variance.

(iii) *Varying AR coefficients and varying noise variance*
If α_m and σ_{Zm} are both allowed to vary with month then one has the persistence given in (2). An examination of (2) shows that if α_m has a minimum at some month m_0, then $P_m(k)$ will tend to have a minimum whenever $(m+k) \geq m_0$. Thus, there will be a drop-off in persistence whenever month m_0 is crossed.

There is also a fourth case of varying AR coefficients and constant noise variance. This case also exhibits a persistence barrier similar to case (iii). As will be seen below, the inclusion of variable noise variance simply allows a closer fit to the observed persistence barrier, but does not qualitatively change the results.

To simulate the NINO3 SST persistence barrier using an autoregressive model, one therefore needs an annual cycle in the AR coefficients. To approximate these coefficients, one can substitute the lag-1 persistences derived from the NINO3 SST into (2) and solve for the AR coefficients:

$$\alpha_m = P_{m-1}(1) \frac{\widetilde{\sigma}_m}{\widetilde{\sigma}_{m-1}}, \tag{3}$$

where the tilde ($\tilde{}$) indicates a quantity from the NINO3 SST data. To estimate $P_{m-1}(1)$ one could use the lag-1 persistences of the NINO3 SST (the black dots in Fig. 2a), but these tend to overestimate the persistence and produce a weak barrier. For a more robust measure of the barrier, the six-month persistence values ($\widetilde{P}_{m-3}(3)$) are used instead. These $\widetilde{P}_{m-3}(3)$ are each assumed to result from a simple AR(1) model, i.e. $\widetilde{P}_{m-3}(3) = [P_{m-1}(1)]^6$, and one can then solve for the "effective" lag-1, $P_{m-1}(1)$. The noise variances are given by $\sigma^2_{Zm} = \widetilde{\sigma}^2_m - \alpha^2_m \widetilde{\sigma}^2_{m-1}$, which is the unexplained variance of each month. The NINO3 persistences and variances, along with the AR coefficients, are given in Table 1.

TABLE 1. Parameters used in the autoregressive model of (1). The lag-6 persistences ($\widetilde{P}_{m-3}(3)$) and variances ($\widetilde{\sigma}_m^2$) are from the NINO3 SST data. The model has lag-1 persistences $P_{m-1}(1)$, AR coefficients α_m, and noise variances σ_{Zm}^2.

	Jan	Feb	Mar	Apr	May	Jun	Jul	Aug	Sep	Oct	Nov	Dec
$\widetilde{P}_{m-3}(3)$	0.47	0.32	0.15	0.08	0.11	0.25	0.39	0.60	0.70	0.70	0.71	0.64
$\widetilde{\sigma}_m^2$ (°C)	0.82	0.63	0.45	0.46	0.42	0.37	0.44	0.53	0.59	0.68	0.84	0.90
$P_{m-1}(1)$	0.88	0.83	0.73	0.66	0.69	0.79	0.85	0.92	0.94	0.94	0.94	0.93
α_m	0.84	0.73	0.62	0.66	0.67	0.74	0.93	1.00	1.00	1.01	1.06	0.96
σ_{Zm}^2 (°C)	0.18	0.20	0.21	0.26	0.22	0.14	0.12	0.08	0.06	0.08	0.09	0.12

This model explains 81% of the NINO3 SST variance (compared with 79% for a simple AR(1) model).

The resulting persistence is shown in Fig. 4a, where we see evidence of a spring persistence barrier caused by the decline in one-month persistence during March–April. During the spring, $\alpha_m < 1$, and random perturbations decay quickly, while during other seasons, $\alpha_m \approx 1$, and the system behaves more like a random walk, with perturbations that can persist and even grow temporarily. These results are similar to those of Blumenthal (1991), who showed that the largest error growth in a principal oscillation pattern (POP) model occurred in February and May. It is encouraging that the model contains growing anomalies similar to growing ENSO modes, yet this growth is constrained by the somewhat arbitrary annual cycle in AR coefficients, rather than any inherent phase locking of ENSO events. The next model that we will consider contains both specified phase locking and typical ENSO events.

(*b*) *Cosine Model*

To simulate the development and structure of actual ENSO events, the following model is now considered:

$$X_t = f_m \gamma_n + Z_t, \tag{4}$$

where m is the month, n is the year, and $t = 12n + m$. In (4), f_m is an idealized ENSO event, γ_n is a three-valued function $\{-1, 0, +1\}$ that sets what type of event will occur that year, and Z_t is a Gaussian white noise process. ENSO events are assumed to last twelve months and have the form,

$$f_m = 2\sin^2((m-3)\pi/12), \tag{5}$$

which starts at zero in April ($m = 3$) and peaks in October ($m = 9$). The occurrence of an event is determined each April by choosing from a uniform random distribution in the range [0, 1] and setting γ_n according to the following probabilities:

$$\gamma_n = \begin{cases} +1 & \text{(Warm event):} \quad 23\% \\ 0 & \text{(no event):} \quad 59\% \\ -1 & \text{(Cold event):} \quad 18\% \end{cases} . \tag{6}$$

These probabilities are derived from the 29 El Niño and 22 La Niña events that took place between 1871–1995 (Kiladis and Diaz 1989).

The monthly variance of (4) is $\sigma_m^2 = \Gamma f_m^2 + \sigma_Z^2$, where $\Gamma = 0.41$ is the total chance of an event occurring and $\sigma_Z^2 = 0.25\ ^\circ\mathrm{C}^2$ is the noise variance. The monthly persistence

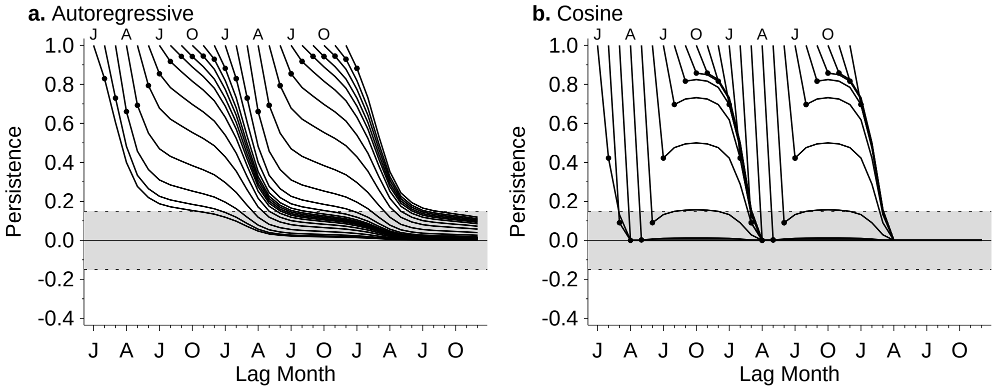

Figure 4. (a) The persistence of the monthly-varying autoregressive model of (1), with coefficients determined from the NINO3 SST data. For comparison with the NINO3 SST persistence, the dotted lines with enclosed shading indicate the 95% confidence levels for Student's-t test with 121 degrees of freedom. The black dots mark the lag-1 persistences. (b) Same as (a) but for the cosine model of (4).

of (4) is

$$P_m(k) = \begin{cases} 1 & k = 0 \\ \dfrac{\Gamma f_m f_{m+k} \delta_{nn'}}{\sigma_m \sigma_{m+k}} & k \geq 1 \end{cases}, \tag{7}$$

where n is the year, n' is the year of month $m+k$, and $\delta_{nn'}$ is zero unless m and $(m+k)$ are in the same April–March year. This persistence is shown in Fig. 4b. For starting months and lags during the same "El Niño" year of April–March, the persistence remains constant. For lags that cross the spring transition the persistence abruptly drops off. Compared to the autoregressive model, this "random ENSO event" model appears to capture more of the essential features of the ENSO cycle, namely, the phase locking of a strong growth-and-decay signal to the annual cycle. This "cosine" model satisfies both parts of the hypothesis and produces a persistence barrier that fits the observed barrier in NINO3 SST and the SOI.

(c) *Signal-to-Noise Ratio*

In case (ii) above, it was shown that an annual cycle of noise variance was unable to explain the persistence barrier in ENSO indices. The AR model with varying coefficients and the "cosine" model with phase-locked events suggest that the persistence barrier is caused by a loss of "information" about conditions following the boreal spring.

The information loss can be parameterized by the signal-to-noise ratio of the system. Figure 5 shows the annual cycle of variance in the NINO3 SST and the signal-to-noise ratio in the AR and "cosine" model. The monthly signal-to-noise is defined for both models as the difference between the total and noise variance divided by the noise variance, i.e.

$$(\text{S:N})_m = \frac{\sigma_m^2 - \sigma_{Zm}^2}{\sigma_{Zm}^2}. \tag{8}$$

If one assumes a constant noise variance for the NINO3 SST, then the monthly variance can also be considered as a measure of the signal-to-noise (but note that low variance by itself does not yield low persistence). All three curves show a minimum in spring, indicating a minimum in "predictive signal". As noted earlier, this loss of information during the spring does not equate to a loss of predictability of the coupled ocean-atmosphere

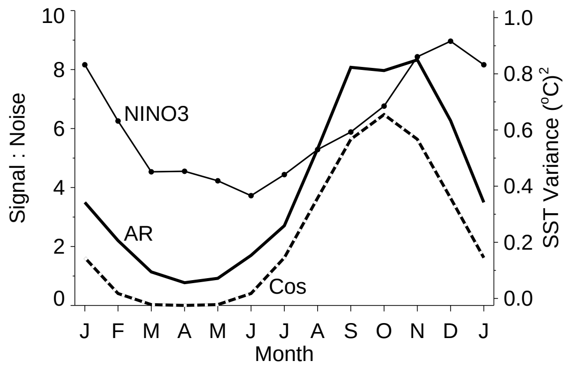

Figure 5. The signal-to-noise ratio (left axis) for the autoregressive (AR) model (solid line) and the cosine (Cos) model (dashed line). The solid line with dots is the annual cycle of NINO3 SST variance from 1871-1996 (right axis).

system. It does, however, imply that coupled models that are limited to the tropical Pacific basin may suffer a decrease in predictive skill from the spring persistence barrier.

(*d*) *Spatial Extent of Persistence*

The success of coupled ocean-atmosphere models for ENSO prediction depends in part on the large spatial extent and high persistence of anomalies in the tropical Pacific. In this section the spatial extent of the persistence barrier is examined and is related to overall forecast skill for the tropics.

Figure 6a shows the six-month seasonal persistence in SST anomalies from June–August (JJA) to the following December–February (DJF). In most of the tropics the persistence is greater than 0.2 (98% significant), while in the core ENSO region in the central Pacific the persistence is greater than 0.4 (99.9% significant). Therefore, given the SST conditions in JJA, this persistence can be used to make useful predictions of DJF conditions over much of the tropics. This persistence is not constant throughout the annual cycle, as shown by the DJF to JJA persistences in Fig. 6b. While the persistence remains above 0.2 over much of the tropics, in the eastern equatorial Pacific the persistence has dropped to near zero. Since this is the region of largest ENSO anomalies, and has the greatest effect on the other tropical regions, a decrease in persistence implies a decrease in predictive skill for the entire tropics.

Other regions of the tropics such as the northern Indian Ocean, the Atlantic, or the south Pacific appear to have moderate persistence, at least for these two seasons. In addition, the persistence in the central Pacific south of the Equator is greater for DJF–JJA than for JJA–DJF, suggesting that there is a migration of high persistence with the annual cycle. It is possible that connections between these high-persistence regions and ENSO could be used to improve forecasts across the spring barrier.

One region that is known to have an impact on the ENSO is the Indian monsoon (Meehl 1987). It has been observed that strong monsoons tend to be followed by cold SST anomalies in the eastern Pacific, and vice versa. Lau and Yang (1996) suggest that models that include the influence of the Asian monsoon on ENSO may be able to use this high Indian Ocean persistence to help bridge the spring Pacific Ocean persistence barrier. The phase difference between the Indian and Pacific Oceans can be seen in a Hovmöller diagram of six-month seasonal persistence along the Equator (Fig. 7a). As expected, the six-month persistence has a strong annual cycle in the eastern Pacific, with

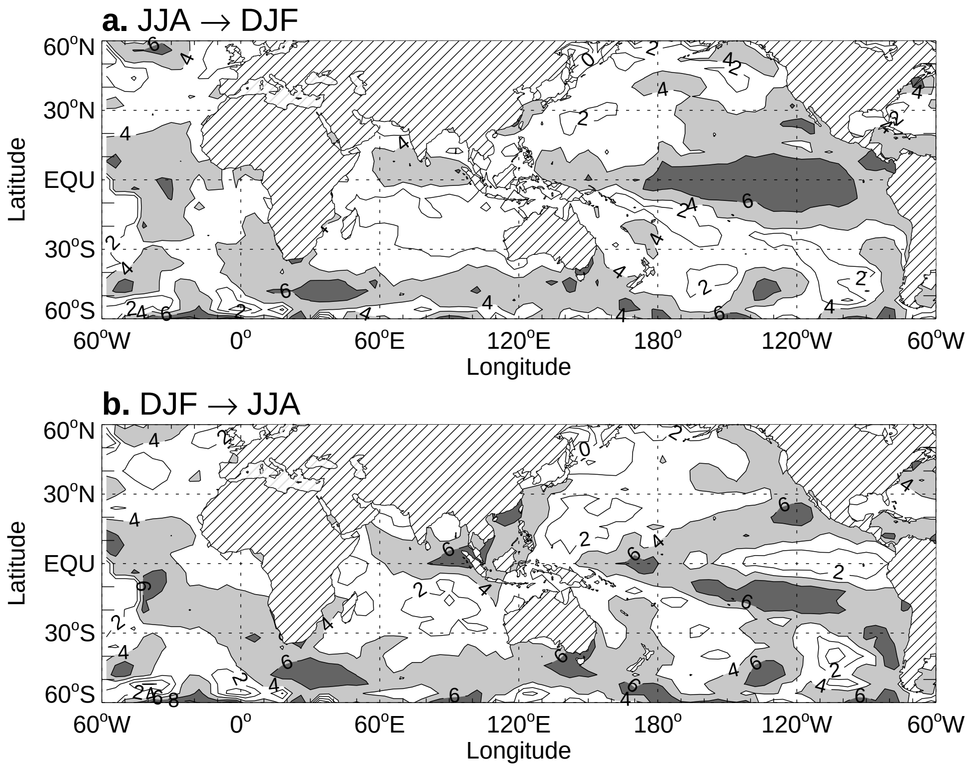

Figure 6. (a) Six-month persistence ($\times 10$) of all June–August (JJA) SST anomalies from 1871–1996 with all the following December–February (DJF) SST anomalies. Contours in persistence are every 0.2 with shading at 0.4 and 0.6. The 95% confidence level is 0.15 for 125 degrees of freedom. (b) Same as (a) but for DJF anomalies correlated with the following JJA anomalies.

the smallest persistence across the spring season. This annual cycle of persistence shows a clear westward progression corresponding to the westward propagation of anomalies in most ENSO events. The most striking feature is the persistence in the eastern Indian Ocean, where the persistence annual cycle is 180°out of phase with the eastern Pacific. In the Indian Ocean, SST anomalies appear to persist from the end of the summer monsoon season, through the following winter, to the beginning of the next monsoon.

It could be argued that the signal in the Indian Ocean is due solely to ENSO effects that have propagated westward. To remove the ENSO signal, the NINO3 SST was linear regressed against each gridpoint at fixed phase (i.e. all January values, then all February, etc.), and this regressed time series was then removed from each point. The fixed-phase regression was used to avoid any artificial signals due to annual cycles in persistence. Figure 7b shows the six-month "non-ENSO" persistence at each gridpoint along the Equator. The persistence in the eastern Pacific has disappeared (along with the annual cycle), but there is still considerable persistence in the Indian Ocean and the western Pacific. A clear semiannual signal is also present in the persistence (with peaks at AMJ and OND), which is perhaps related to the semiannual cycle of insolation on the Equator.

The above results suggest that the large persistence across much of the tropics can be used to improve model forecast skill. At the same time, information outside of the eastern Pacific may be helpful in bridging the spring persistence barrier.

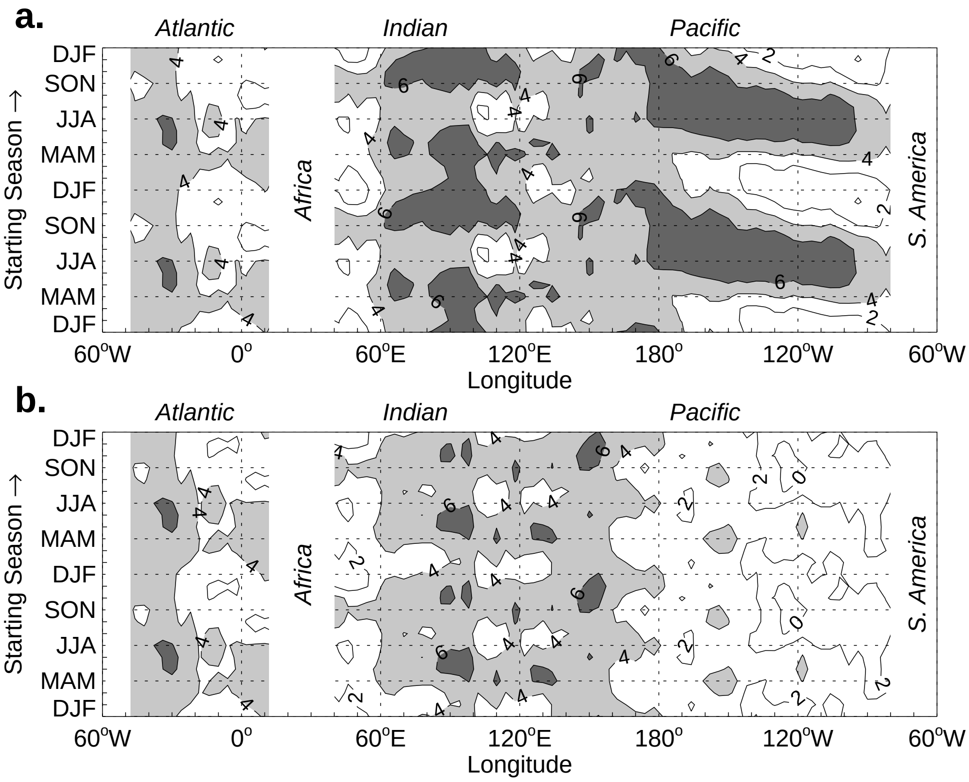

Figure 7. (a) Annual cycle of six-month persistence ($\times 10$) of SST anomalies at each point along the Equator. The method is the same as in Fig. 6. The y-axis indicates the starting month and the cycle has been repeated. Contours are every 0.2, with shading at 0.4 and 0.6. The vertical white bands indicates land. (b) Same as (a) but with the NINO3 SST signal removed from each gridpoint, using a fixed-phase regression of monthly NINO3 SST onto each point.

5. Interdecadal Variability

(*a*) *Interdecadal Changes in Variance*

Improvements to model forecasts such as that shown for the Cane-Zebiak model (Chen *et al.* 1995), as well as results from statistical analyses, must be viewed in the context of longer-term variability. Both the Asian monsoon and ENSO have undergone significant interdecadal changes in the past 100 years (Parthasarathy *et al.* 1991; Trenberth 1976).

Using wavelet and waveform analysis, Wang and Wang (1996) showed that east Pacific SST and Darwin SLP underwent considerable interdecadal variability. Specifically, periods from 1875–1920 and 1960–1990 showed high ENSO variance, while 1920–1950 showed low ENSO variance. Gu and Philander (1995) show similar changes in the zonal winds. However, Wang and Wang's analysis also showed reduced wavelet power before 1950, possibly due to the sparseness and decreased reliability of the pre-1950 data from COADS (Comprehensive Ocean-Atmosphere Data Set; for data quality issues see Folland *et al.* 1984).

To quantify and isolate the time scales involved in these variance changes, the NINO3 SST, the SOI, and the Indian rainfall time series were decomposed using a wavelet transform. The wavelet transforms were then scale-averaged between 2–8 years, to produce a

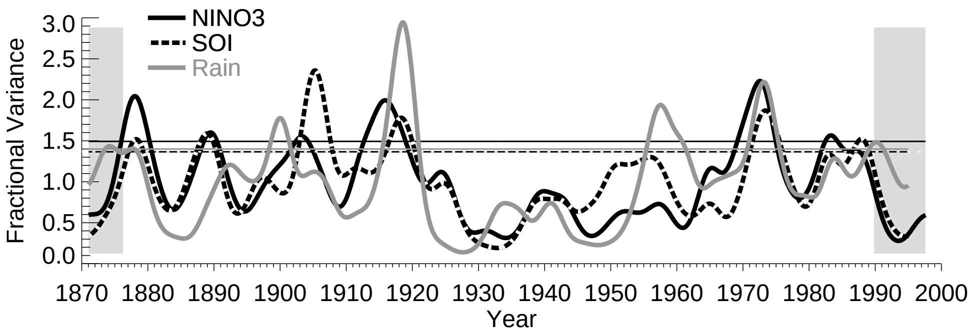

Figure 8. Average wavelet power in the 2–8 year band for the NINO3 SST (solid), the GMSLP SOI (dashed), and the Indian rainfall (gray). Each curve was normalized by dividing by its mean. The gray bands indicate where zero-padding has reduced the variance. The thin lines are the 95% confidence levels, assuming red noise of lag-1=0.89 for NINO3, lag-1=0.62 for SOI, and lag-1=0.0 for Indian rainfall.

time series of variance in the ENSO frequency band. For details of the wavelet analysis, including the derivation of significance levels, see Torrence and Compo (1998).

Figure 8 shows the time series of 2–8 year variance for NINO3 SST, the SOI, and Indian rainfall. The variance in all three indices shows a long-period change, with high variance between 1875–1920, low variance from 1920–1950 and then high variance from 1960–1990. The new significance tests indicate that these long-period variance changes are statistically significant (Torrence and Compo 1998). The use of the GISST2.3 dataset appears to increase the reliability of the pre-1950 NINO3 SST, and suggests that the pre-1920 period has equal power to the post-1960 period. In addition to the period of low variance during 1920–1950, there appears to be a 15-year oscillation in variance. This 15-year "oscillation" may be due to the occurrence of extreme ENSO events, which tend to recur every 8–11 years.

(*b*) *Interdecadal Changes in Persistence*

The interdecadal variability shown in Fig. 8 should be reflected in the persistence, with periods of low ENSO variance (1920–1950) associated with small persistence, and periods of high variance associated with large persistence. The persistence for 1871–1920 is shown in Fig. 9a, and appears similar to the persistence for the entire time series in Fig. 2. The persistence for 1920–1950 (Fig. 9b) is much lower and has less of a barrier compared to either the earlier or later period

The most recent period can be further divided as shown in Figs. 9c and 9d: the 1960–1977 period shows strong phase locking of persistence to the annual cycle, while the 1978–1995 period shows very little phase locking of persistence.. Using a running three-month persistence, Balmaseda *et al.* (1995) found similar changes between all four periods. As discussed in the next section, this change in persistence phase locking can be related to changes in the phase locking of ENSO events.

6. DISCUSSION

(*a*) *Model Forecast Skill*

A spring predictability barrier is seen in the skill of models attempting to predict tropical interannual variability (Barnston *et al.* 1994). Four of the five models used in

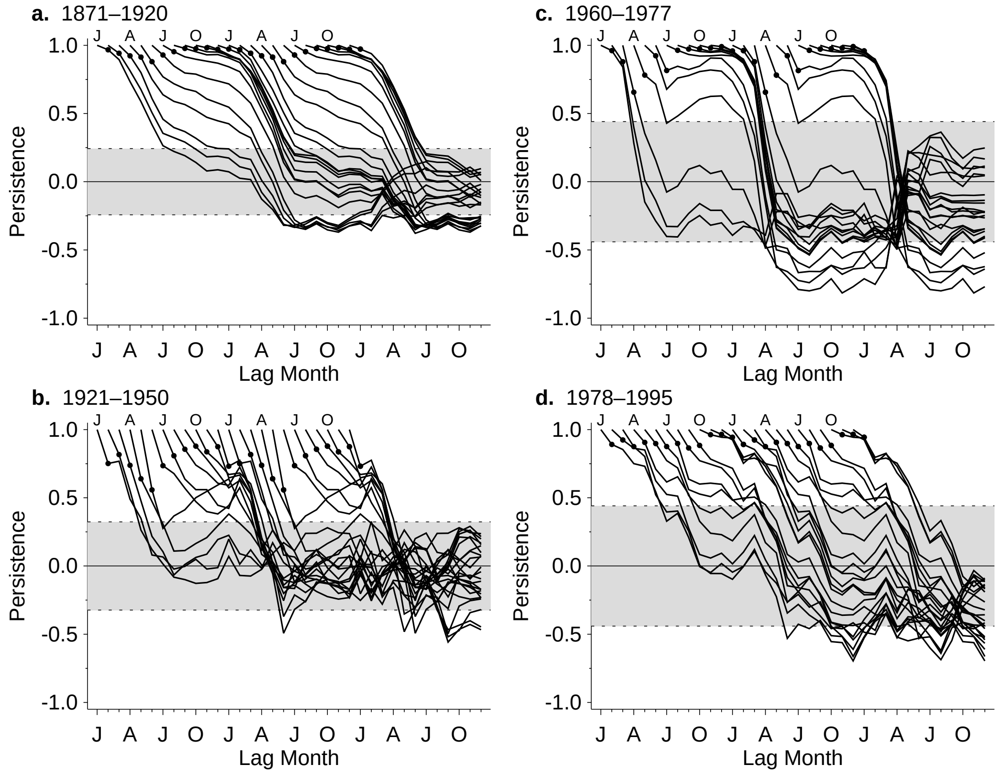

Figure 9. Monthly persistence plots for various subsets of the 1896–1995 NINO3 SST data. See Fig. 2 for details. (a) Persistence using only 1896–1920 (25 years), (b) 1921–1950 (30 years), (c) 1960–1977 (18 years), (d) 1978–1995 (18 years).

Barnston *et al.* show the lowest skill when predicting anomalies for the summer (June–August) season. These four also have the largest root-mean-square error (RMSE) between observed and predicted SST for spring (March–May) or summer forecasts. The only exception is the NOAA/NCEP coupled model (Ji *et al.* 1994), which has the lowest correlation and highest RMSE for fall (September–November) forecasts initiated in the previous winter (December–February). This is possibly due to the inclusion of subsurface ocean temperatures in the model initialization, which may improve the short-range forecasts and delay the skill drop-off. All five models have the highest correlation and lowest RMSE when predicting the winter season for forecasts initiated in the previous spring.

Xue *et al.* (1994) attribute the decline in model forecast skill across the spring to the low variance of the NINO3 SST anomalies during March–May. Defining the mean-square error (MSE) between the observed SST's, X, and the forecasts, Y, as $\mathrm{MSE} = \langle (X - Y)^2 \rangle$, where $\langle \bullet \rangle$ indicates the mean, they show that the correlation between X and Y can be written as:

$$r = \frac{\langle XY \rangle}{\sigma^2} = 1 - \frac{\mathrm{MSE}}{2\sigma^2}, \tag{9}$$

where it has been assumed that the standard deviation σ is the same for both X and Y. Xue *et al.* assume that the MSE is constant, and then conclude that the annual cycle in NINO3 variance (with a spring minimum), should produce a spring persistence barrier. As noted by Xue *et al.*, however, the MSE is also lowest in the spring, and hence it is unclear which one is the dominant term. The dilemma is solved by noting that the

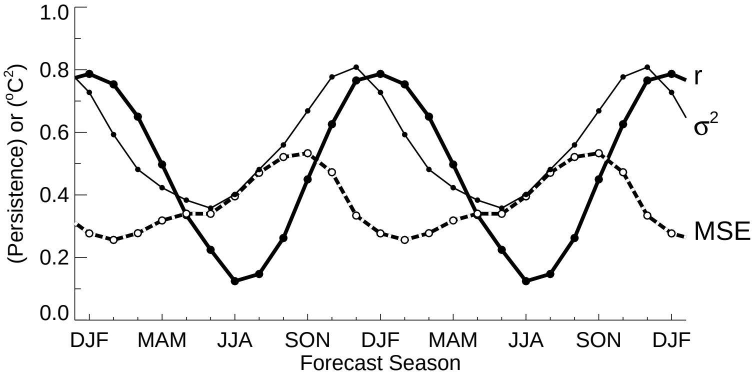

Figure 10. Results for forecasts of NINO3 SST (3-month running averaged) using six month persistence. The x-axis is the forecast season, and the time series are repeated for clarity. The time series are the persistence r (thick line), the variance (σ^2) of NINO3 SST for the forecast season (in $^\circ C^2$; thin line), and the mean-square error (MSE) between the forecast and the observed data (in $^\circ C^2$; dashed line).

correlation, mean-square error, and standard deviation are all functions of X and Y and should not be thought of as independent quantities. If X and Y are each normalized by their own standard deviation, then the correlation becomes,

$$r = 1 - \frac{1}{2}(\mathrm{MSE})', \tag{10}$$

where $(\mathrm{MSE})'$ is the mean-square error of the normalized variables. This normalized mean-square error is smallest for winter forecasts and largest for summer forecasts, at least for the full Cane-Zebiak model (Barnston *et al.* 1994).

An example of the relationship between r, MSE, and σ^2 is given in Fig. 10, which shows the persistence forecast for NINO3 SST with a six-month lead. Beginning with DJF forecasts, the persistence (or forecast skill) slowly drops off across the spring season to reach a minimum for forecasts of JJA temperatures. Both the decreasing variance of the forecast season and the increasing mean-square error contribute to the drop-off in persistence (in addition to the different variance between the starting and forecast season, which can no longer be ignored). Because of the annual cycle of MSE, the persistence r lags the variance σ^2 by about one month. These results are also in agreement with Section 4, where it was shown that an annual cycle in the signal-to-noise ratio could produce a persistence barrier, while an annual cycle in noise variance could not.

The annual cycle of variance is therefore a *result* of the spring season being the transition time between warm and cold events, while the predictability barrier in forecast skill can be attributed to the large *normalized* mean-square error during the spring season.

(*b*) *Persistence vs. Predictability*

It is important to note that any time series derived from the phase-locked ENSO signal will tend to show an annual cycle in its statistics. For example, if a coupled ocean-atmosphere model shows phase locking of ENSO events to the annual cycle, then an analysis of forecast skill using model-predicted NINO3 SST will contain a spring barrier. In analyzing the skill of a model, it would thus be better to use some sort of global measure rather than a single time series.

The presence of a persistence barrier in a time series does not indicate a true predictability barrier of the whole system. Both the NINO3 SST and the SOI are limited-area indices of a global-scale phenomenon. There are certainly many precursors to anomalies in these time series (Rasmusson and Carpenter 1982), and changes in global circulation may cause changes in the importance of these indices as indicators of ENSO variability (Trenberth 1976). In addition, persistence itself relies on the assumption of linearity, and may not be the most appropriate measure for predictability.

Recent model results by Penland and Sardeshmukh (1995) and Chen *et al.* (1995) suggest that the the inclusion of other variables and improved parameterizations, as well as better initialization, might be able to circumvent the barrier. In both of these models, one statistical and the other dynamical, the input (or training) data is smoothed by the initialization process. This smoothing filters out any high-frequency noise that could otherwise project onto the ENSO modes. Neither of these models shows a significant spring barrier, however, the interdecadal changes in variance may be masking the influence of the barrier on ENSO forecasts.

(*c*) *Interdecadal Changes & Predictability*

The results of Section 5 indicate that ENSO undergoes interdecadal changes in both variance and persistence. Given the changes in both persistence and forecast skill on interdecadal time scales, it is unclear whether the predictability barrier has indeed been “eliminated” in the Cane-Zebiak model (Chen *et al.* 1995). It is possible that the weaker phase locking of ENSO to the annual cycle during the 1980’s might remove any seasonality in forecast skill.

Using a coupled ocean-atmosphere model, Balmaseda *et al.* (1995) show that there is a spring barrier to SST forecast skill, and that this forecast skill has considerable interdecadal variability. During the 1970’s the ENSO variability was strongly phase locked to the annual cycle, and there was a strong predictability barrier. During the 1980’s and 1990’s the ENSO variability has not been phase locked to the annual cycle, the predictability barrier was much weaker, and the overall forecast skill was higher than the 1970’s.

Wang (1995) showed that, prior to 1980, ENSO events started in the eastern Pacific and migrated west, while those after 1980 started in the central Pacific and were stationary. The 1970’s period shows strong equatorial trade winds and low SST’s, while the 1980’s show weak trades and higher SST’s (Wang 1995; Clarke and Lebedev 1996). This warming of the eastern Pacific since 1980 and the weakening of the trade winds might decrease the dependence of El Niño onset on the phase of the annual cycle, and could also explain the prolonged 1991–1995 “warm event”.

For the improved Cane-Zebiak model (Chen *et al.* 1995), the model forecast skill increased for the 1980’s but not for the 1970’s. Since the 1980’s had less of a persistence barrier than the 1970’s, one would expect that an increase in forecast skill for the 1980’s would decrease the apparent strength of the spring barrier for the entire 1972–1992 period, as was found in their results.

The presence of the persistence barrier and the interdecadal changes in variance have three implications for ENSO modeling:

(i) Claims of significant improvements in ENSO forecasting must be related to persistence and variance during the particular time period,
(ii) The current persistence barrier strength and the ENSO variance should be used to establish confidence levels for ENSO forecasts, and
(iii) The causes of interdecadal changes in predictive skill and variance should be identified, and if possible, incorporated into coupled ocean-atmosphere models.

It is hoped that through the use of measures of the persistence and variance, it will be possible to improve the reliability and extent of ENSO forecasts.

7. Summary

A predictability barrier has been shown to exist in statistical analyses of ENSO variability. The barrier is seen as a persistence drop-off during the spring (March–May) in statistical analyses, and as a forecast skill decline in many numerical models (Barnston *et al.* 1994). The barrier's existence has been questioned as an artifact of the statistical analysis, with the suggestion that the annual cycle of ENSO variance is responsible for the annual cycle of skill (Xue *et al.* 1994).

Using simple statistical models of ENSO indices, it was shown that the annual cycle of the signal-to-noise ratio is responsible for the persistence barrier. The phase locking of ENSO to the annual cycle is the cause of the persistence barrier, while the minimum in variance in spring is a result of this phase locking.

The strength of the persistence barrier and the ENSO variance were shown to vary on interdecadal time scales. The changes in ENSO variance were shown to be correlated to changes in Indian monsoon rainfall variance. From 1871–1920 and 1960–1977 the ENSO variance was high and the persistence barrier was strong while from 1921–1950 the ENSO variance was low and the persistence barrier was weak. Finally, from 1960–1977 the persistence barrier was strong and the ENSO events were phase locked to the annual cycle, while from 1978–1995 the persistence barrier was weak and the ENSO events showed little phase locking.

Areas of future research include quantifying the relationship between the persistence barrier in ENSO indices and model forecast skill, defining useful confidence levels for ENSO forecasts, and identifying the causes of interdecadal changes in the coupled ocean-atmosphere system.

Appendix

The monthly persistence of a time series X_t is defined as the covariance of the two sets of months divided by their standard deviations. For months m and $m+k$, where k is the lag, the persistence is thus:

$$P_m(k) = \frac{\sigma^2_{m,m+k}}{\sigma_m \sigma_{m+k}}. \tag{A.1}$$

The covariance and variance are at fixed phase with respect to the annual cycle, i.e.,

$$\sigma^2_{m,m+k} = \frac{1}{N-1} \sum_{n=0}^{N-1} X_{12n+m} X_{12n+m+k} \tag{A.2}$$

$$\sigma^2_m = \frac{1}{N-1} \sum_{n=0}^{N-1} X^2_{12n+m}, \tag{A.3}$$

where we have assumed that the monthly means of X_t are zero. Index m is the month, n is the year, while t is the time index such that $t = 12n + m$. For the autoregressive model, $X_t = \alpha_m X_{t-1} + Z_t$, the monthly variance is:

$$\sigma^2_m = \sigma^2_{Zm} + \alpha^2_m \sigma^2_{m-1} \tag{A.4}$$

where σ^2_{Zm} is the variance for the m-th month of the noise, and we have used the assumption that the noise is uncorrelated with itself to eliminate the cross term.

Using recursive substitution, (A.4) can be rewritten as:

$$\begin{aligned}\sigma^2_m &= \sigma^2_{Zm} + \alpha^2_m \sigma^2_{Zm-1} + \alpha^2_m \alpha^2_{m-1} \sigma^2_{Zm-2} + \ldots + \sigma^2_{Zm-11} \prod_{j=0}^{10} \alpha^2_{m-j} \\ &\quad + A^2 \sigma^2_{m-12}, \end{aligned} \tag{A.5}$$

where $A = \prod_{j=0}^{11} \alpha_j$ is a constant equal to the product of all 12 AR coefficients. In the last term in (A.5) we have $\sigma^2_{m-12} = \sigma^2_m$ and the recursion repeats itself, with each set of 12 terms reduced by another factor of A^2. Note also that there are twelve of these equations, one for each month. For convergence we require $A < 1$, and the infinite sums in A^2 can be reduced as,

$$\sigma^2_m = \frac{1}{1 - A^2} \sum_{m'=0}^{11} \sigma^2_{Zm-m'} \prod_{j=0}^{m'-1} \alpha^2_{m-j}, \tag{A.6}$$

where $\prod_{j=0}^{-1} \alpha^2_{m-j} \equiv 1$. Thus the monthly variance of our model is a combination of all the previous noise variances weighted by the AR coefficients.

To derive the covariance, the time series (1) is first rewritten as:

$$X_{12n+m+k} = Z_{12n+m+k} + \alpha_{m+k} Z_{12n+m+k-1} + \ldots + X_{12n+m} \prod_{j=1}^{k} \alpha_{m+j}. \tag{A.7}$$

When this is substituted into (A.2) all of the noise terms are eliminated while the X_{12n+m} term gives:

$$\sigma^2_{m,m+k} = \sigma^2_m \prod_{j=1}^{k} \alpha_{m+j}. \tag{A.8}$$

Substituting (A.8) into (A.1) gives the persistence for the AR model,

$$P_m(k) = \frac{\sigma_m}{\sigma_{m+k}} \prod_{j=1}^{k} \alpha_{m+j}, \tag{A.9}$$

with the monthly variances given by (A.6). The persistence for the "cosine" model of (4) can be derived in a similar manner.

Acknowledgements

Thanks to Drs. G. Compo, R. Tomas and J. Weiss of PAOS, and Dr. C. Penland of CDC for many useful discussions on predictability and wavelet analysis. Computing was done at the PAOS Computer Facility. This work was funded by grant NA56GP0230 of the NOAA Office of Global Programs.

References

Balmaseda, M. A., Anderson, D. L. T., and Davey, M. K. 1994 ENSO prediction using a dynamical ocean model coupled to statistical atmospheres, *Tellus*, **46A**, 497–511.

Balmaseda, M. A., Davey, M. K., and Anderson, D. L. T. 1995 Decadal and seasonal dependence of ENSO prediction skill, *J. Climate*, **8**, 2705–2715.

Barnett, T. P.	1991	The interaction of multiple time scales in the tropical climate system, *J. Climate*, **4**, 269–285.
Barnston, A. G., van den Dool, H. M., Zebiak, S. E., Barnett, T. P., Ji, M., Rodenhuis, D. R., Cane, M. A., Leetmaa, A., Graham, N. E., Ropelewski, C. R., Kousky, V. E., O'Lenic, E. A., and Livezey, R. E.	1994	Long-lead seasonal forecasts - where do we stand?, *Bull. Amer. Meteor. Soc.*, **75**, 2097–2114.
Blumenthal, M. B.	1991	Predictability of a coupled ocean-atmosphere model, *J. Climate*, **4**, 766–784.
Cane, M. A., Zebiak, S. E., and Dolan, S. C.	1986	Experimental forecasts of El Niño, *Nature*, **321**, 827–832.
Chen, D., Zebiak, S. E., Busalacchi, A. J., and Cane, M. A.	1995	An improved procedure for El Niño forecasting, *Science*, **269**, 1699–1702.
Chen, D., Zebiak, S. E., Cane, M. A., and Busalacchi, A. J.	1997	Initialization and predictability of a coupled ENSO forecast model, *Mon. Wea. Rev.*, **125**, 773–788.
Clarke, A. J. and Lebedev, A.	1996	Long-term changes in the equatorial Pacific trade winds, *J. Climate*, **9**, 1020–1029.
Folland, C. K., Parker, D. E., and Kates, F. E.	1984	Worldwide marine temperature fluctuations 1856–1981, *Nature*, **310**, 670–673.
Goswami, B. N. and Shukla, J.	1991	Predictability of a coupled ocean-atmosphere model, *J. Climate*, **4**, 3–22.
Gu, D. and Philander, S. G. H.	1995	Secular changes of annual and interannual variability in the tropics during the past century, *J. Climate*, **8**, 864–876.
Ji, M., Kumar, A., and Leetmaa, A.	1994	An experimental coupled forecast system at the National Meteorological Center: Some early results, *Tellus*, **46A**, 398–418.
Kiladis, G. N. and Diaz, H. F.	1989	Global climatic anomalies associated with extremes in the Southern Oscillation, *J. Climate*, **2**, 1069–1090.
Latif, M. and Graham, N. E.	1991	How much predictive skill is contained in the thermal structure of an OGCM?, *TOGA Notes*, **2**, 6–8. Nova Southeastern University, Oceanographic Center, 8000 North Ocean Drive, Dania, Florida 33004, U.S.A.
Lau, K.-M. and Yang, S.	1996	The Asian monsoon and predictability of the tropical ocean-atmosphere system, *Quart. J. Roy. Meteor. Soc.*, **122**, 945–957.
Meehl, G. A.	1987	The annual cycle and interannual variability in the tropical Pacific and Indian ocean regions, *Mon. Wea. Rev.*, **115**, 27–50.
Mooley, D. A. and Parthasarathy, B.	1984	Fluctuations in all-India summer monsoon rainfall during 1871–1978, *Clim. Change*, **6**, 287–301.
Moore, A. M. and Kleeman, R.	1996	The dynamics of error growth and predictability in a coupled model of ENSO, *Quart. J. Roy. Meteor. Soc.*, **122**, 1405–1446.
Normand, C.	1953	Monsoon seasonal forecasting, *Quart. J. Roy. Meteor. Soc.*, **79**, 463–473.
Parthasarathy, B., Kumar, K. Rupa, and Munot, A. A.	1991	Evidence of secular variations in Indian monsoon rainfall-circulation relationships, *J. Climate*, **4**, 927–938.
Penland, C. and Sardeshmukh, P. D.	1995	The optimal growth of tropical sea surface temperature anomalies, *J. Climate*, **8**, 1999–2024.
Rasmusson, E. M. and Carpenter, T. H.	1982	Variations in tropical sea surface temperature and surface wind fields associated with the Southern Oscillation/El Niño, *Mon. Wea. Rev.*, **110**, 354–384.

Rayner, N. A., Horton, E. B., Parker, D. E., Folland, C. K., and Hackett, R. B. 1996 Version 2.2 of the Global sea-Ice and Sea Surface Temperature data set, 1903–1994, Technical report, CRTN 74, Hadley Centre for Climate Prediction and Research, Meteorological Office, London Road, Bracknell, Berkshire, RG12 2SY, 21 pp.

Ropelewski, C. F. and Jones, P. D. 1987 An extension of the Tahiti-Darwin Southern Oscillation index, *Mon. Wea. Rev.*, **115**, 2161–2165.

Torrence, C. and Compo, G. P. 1998 A practical guide to wavelet analysis, *Bull. Amer. Meteor. Soc.*, **79**, 61–78.

Treloar, H. M. and Grant, A. M. 1953 Some correlation studies of Australian rainfall, *Aust. J. Agricultural Res.*, **4**, 423–429.

Trenberth, K. E. 1976 Spatial and temporal variations of the Southern Oscillation, *Quart. J. Roy. Meteor. Soc.*, **102**, 639–653.

Trenberth, K. E. 1984 Signal versus noise in the Southern Oscillation, *Mon. Wea. Rev.*, **112**, 326–332.

Troup, A. J. 1965 The "southern oscillation", *Quart. J. Roy. Meteor. Soc.*, **91**, 490–506.

Walker, G. T. and Bliss, E. W. 1932 World weather V, *Mem. Roy. Meteor. Soc.*, **4**, 53–84.

Walker, G. T. and Bliss, E. W. 1937 World weather VI, *Mem. Roy. Meteor. Soc.*, **4**, 119–139.

Wang, B. 1995 Interdecadal changes in El Niño onset in the last four decades, *J. Climate*, **8**, 267–285.

Wang, B. and Wang, Y. 1996 Temporal structure of the Southern Oscillation as revealed by waveform and wavelet analysis, *J. Climate*, **9**, 1586–1598.

Webster, P. J. 1995 The annual cycle and the predictability of the tropical coupled ocean-atmosphere system, *Meteor. Atmos. Phys.*, **56**, 33–55.

Webster, P. J. and Yang, S. 1992 Monsoon and ENSO: Selectively interactive systems, *Quart. J. Roy. Meteor. Soc.*, **118**, 877–926.

Wright, P. B. 1979 Persistence of rainfall anomalies in the central Pacific, *Nature*, **277**, 371–374.

Wright, P. B. 1985 The Southern Oscillation: An ocean-atmosphere feedback system?, *Bull. Amer. Meteor. Soc.*, **66**, 398–412.

Wright, P. B. 1987 Variations in tropical Atlantic sea surface temperatures and their global relationships, Report 12, Max Planck Institut für Meteorologie, Bundesstrasse 55, 2000 Hamburg 13, Germany.

Xue, Y., Cane, M. A., Zebiak, S. E., and Blumenthal, M. B. 1994 On the prediction of ENSO: A study with a low-order markov model, *Tellus*, **46A**, 512–528.